Interplay between Single and Cooperative H 2 Adsorption in the Saturation of Defect Sites at MgO Nanocubes

Francia Haque, Fabio Finocchi, Stéphane Chenot, Jacques Jupille, Slavica Stankic, Camille Simon, Valentina Caorsi, Clément Campillo, C. Sykes

Interplay between Single and Cooperative H_2 Adsorption in the Saturation of Defect Sites at MgO Nanocubes

Francia Haque, Fabio Finocchi, Stephane Chenot, Jacques Jupille, and Slavica Stankic*

Sorbonne Université, CNRS, Institut des NanoSciences de Paris, INSP, F-75005 Paris, France

Supporting Information

ABSTRACT: The configurations associated with reversible and irreversible adsorption of hydrogen on MgO escape consensus. Here, we report the dissociation of H_2 on MgO nanocubes, which was examined by combining Fourier transform infrared spectroscopy and density functional theory (DFT)-based simulations. We found that the use of ultrahigh vacuum is essential for identifying the very first adsorption stages. Hydrogen pressure was varied from 10^{-8} mbar to near ambient, resulting in IR spectra of richer complexity than in current state of the art. Models with oxygen at regular corners (O_{3C}) and Mg at inverse corners (Mg_{IC}) were identified to be the most reactive and to split H_2 irreversibly already in the lowest pressure regime ($P_{H_2} < 10^{-3}$ mbar). The continuous increase in intensity of the corresponding IR bands (3712/1140 cm^{-1}) in the intermediate range of pressures (10^{-3}–1 mbar), along with the appearance of bands at 3605/1225 cm^{-1}, was demonstrated to stem from cooperative adsorption mechanisms, which could be therefore considered as the main origin of irreversible hydrogen adsorption. At $P_{H_2} > 1$ mbar, fully reversible adsorption was shown to occur at O_{4C} (either on mono- or diatomic steps) and Mg_{3C} sites. Another OH/MgH couple (3697/1030 cm^{-1}) that became reinforced at high P_{H_2} but remained stable upon pumping was correlated to O_{3C} and Mg_{IC} in multiatomic steps. The difference in adsorption and desorption sequences confirmed the proposed cooperative adsorption of H_2 molecules. Our study provides new insights into the mechanisms that can be beneficial for understanding the chemistry of H_2 and other hydrogen-containing molecules, such as CH_4, on oxide surfaces, but also for the advancement of hydrogen-storage technologies.

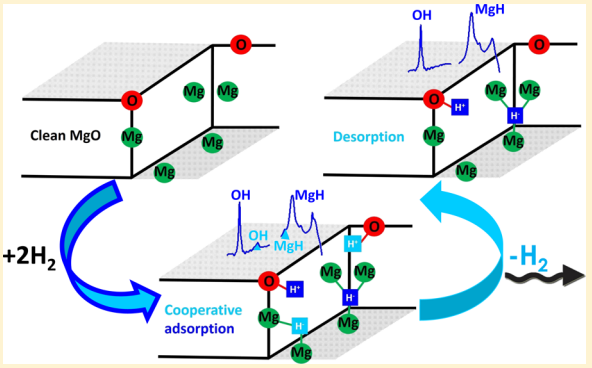

1. INTRODUCTION

Understanding hydrogen adsorption and dissociation on oxide surfaces is central to unraveling many chemical and physical processes that involve hydrogen-containing molecules. A better comprehension of mechanisms for hydrogen storage is also necessary as to meet hydrogen storage requirements established by the Department of Energy. The prototypical system for studying the hydrogen interaction with oxide surface sites is represented by MgO nanocrystals. The formation of hydroxyl and hydride groups, as evidenced by infrared spectroscopy upon interaction of hydrogen with MgO powders, was first assigned to H^+/H^- heterolytic dissociation on low-coordinated O^{2-}/Mg^{2+} pairs, respectively.[1] This experimental study was followed by a series of computational works[2−5] in which the chemical activity of MgO surface atoms was found to be in a strong correlation with their coordination number. In particular, at least one 3-coordinated site was judged as necessary for a stable hydrogen adsorption on the MgO surface.[6] On highly dispersed MgO, two H_2-adsorption channels were identified to give rise for OH/MgH stretching vibrations with frequencies at 3712/1125 and 3460/1325 cm^{-1}.[7] In the same study, the former couple was observed to be irreversible upon H_2 evacuation and was assigned to homolytic H_2-splitting, a process that should involve paramagnetic O^-/Mg^+ species. Later, however, an electron paramagnetic resonance-based study discarded the existence of such species on a clean MgO surface and demonstrated that both of the IR-detected OH/MgH couples must stem from heterolytic dissociation processes.[8] At $P_{H_2} \geq 1$ mbar, the irreversible OH/MgH couple was observed to reach its saturation limit, whereas the second one (3460/1325 cm^{-1}) starts growing at this pressure and can be completely removed upon H_2 evacuation, being, thus, referred as reversible.[7,8]

Many efforts have been invested to establish a correlation between the two above-mentioned H_2 adsorption processes and appropriate surface configurations. 3-Coordinated Mg−O pairs ($Mg_{3C}O_{3C}$) including subsequent stabilization by H-bonding were first suggested by Knözinger et al.[7] To explain the irreversible adsorption, H^- was proposed to adsorb at an inverse corner where it is shared between three Mg ions along with H^+ being adsorbed at neighboring O_{4c}.[9−11] The bonding of H^- at an inverse corner was then extended to the crossing

point of two monoatomic steps (H^- being bonded to two Mg_{4C} and one Mg_{5C}) in combination with a O_{4c}–H^+ moiety.[10] The reversible dissociative adsorption was attributed to O_{4c} and Mg sites on two neighboring ⟨100⟩ steps[9] or by placing the H^+ ion on the O_{5C} atom situated at the bottom of the inverse corner.[10] Finally, in ref 11, the irreversible adsorption of H^+/H^- fragments was associated with O_{3C} and Mg_{IC} (two Mg_{4C} and one Mg_{5C}) sites. For reversible adsorption, this group of authors put forward an oxygen inverse corner in which H^+ is shared between three O_{5C} atoms and H^- sitting shared between two adjacent Mg_{5C} atoms. Among quite different surface structures reported so far, a common point is the key role suggested for inverse corners.[7,9−11] These interpretations, with the exception of the work by Ricci et al.[10] and Cavalleri et al.,[12] are solely based on experimental data. The proposed configurations vary mainly regarding the coordinate number of the anions (or cations) of which the corresponding inverse corner is build. Although the nature of the sites that are involved in H_2 is still controversial, a systematic approach combining theory and experiments is lacking. Moreover, on the experimental side, the partial pressures of hydrogen that have been used range between 1 and 100 mbar, which does not allow us to test the stability of the observed configurations over a large pressure range.

The present work reports on a combined Fourier transform infrared (FTIR) study and first-principles calculations on H_2 adsorption at MgO surface. MgO nanocrystals were synthesized via chemical vapor synthesis (CVS) to provide high surface area (≥300 $m^2\ g^{-1}$) with a significant contribution of defects such as steps, edges, corners, and inverse steps and corners. Adsorption of H_2 was probed at partial pressures ranging from ultrahigh vacuum (UHV) (10^{-8} mbar) to almost ambient (100 mbar) to allow the determination of the pressure threshold. The objective is to identify microscopic H^+/H^- adsorption sites via frequencies and adsorption free energy estimated by ab initio calculations.

2. METHODS

2.1. Synthesis and FTIR Measurements. Measurements have been performed in a UHV apparatus involving a preparation chamber and a main chamber, both including working pressure in the 10^{-10} mbar range. Fourier transform infrared (FTIR) spectroscopy was performed on MgO pellets in the main chamber (through ZnSe windows) in the transmission mode by means of a Bruker Vertex 70 FTIR spectrometer equipped with a MCT detector. Blanks were collected prior to exposure and used as references. MgO powders were obtained via the CVS technique.[13] The specific surface area of the resulting MgO material is 365 $m^2\ g^{-1}$ as determined by Brunauer–Emmett–Teller (LN_2) measurements. Transmission electron microscopy (TEM) analysis of the particles was achieved using a JEOL 2100 field emission transmission electron microscope operated at 200 kV with a 0.18 nm resolution. The statistics used to plot particle size distribution involved an observation of more than 300 particles. As a starting material, high-purity Mg pieces (>99.98%) supplied by Goodfellow were used. The CVS-MgO powder was pressed into pellets with an applied pressure of less than 5 bar to avoid any changes in the specific surface area. Prior to being transferred in the main analysis chamber, MgO pellets were degassed at 1170 K in UHV for 1 h in the preparation chamber. The applied annealing treatment guaranties adsorbate-free MgO surfaces, which was confirmed by the absence of any adsorbed impurity in the initial infrared spectrum of MgO only. Reference spectra used for the subtraction were recorded on the degassed MgO pellet in UHV. Hydrogen that was used for adsorption was supplied by Air Liquide with purity 99.999%. The IR spectra were recorded with a resolution of 4 cm^{-1} by averaging 250 interferogram scans to obtain a reasonable signal-to-noise ratio.

2.2. Density Functional Theory (DFT) Calculations. The calculations were performed using the Quantum Espresso program suite,[14] within the generalized gradient approximation (Perdew–Burke–Ernzerhof)[15] to density functional theory (DFT).[16] We accounted for the interaction between the ionic cores and the valence electrons by ultrasoft pseudopotentials (see Supporting Information for details).

The periodic slabs are at least seven atomic (001) layer thick, with one or two fixed central layers and a large enough void space. The defect sites were simulated through the use of shifted periodic boundary conditions: first, we built up the MgO(001) slabs. We then adopted peculiar base vectors to represent vicinal (01n) or (02n) surfaces (n = 5−7), with mono- or diatomic steps, and 4-fold-coordinated atoms on the ledge.[17] To simulate defects with lower coordination numbers, we applied shifted periodic boundary conditions along the step direction, too. In this way, we could simulate corners and reverse corners on mono- and diatomic steps on MgO surfaces (Figure 1).

We studied other models for H_2 splitting, such as MgO(011) surfaces, which show straight ledges with an equal number of O and Mg ions along the [100] direction. We also considered point defects, such as MgO divacancies in variable number NV_{MgO} (NV_{MgO} = 1−3) on terraces and monoatomic steps, as they are active sites for the dissociation of water and other molecules.[18] Overall, we examined almost a hundred nonequivalent adsorption configurations.

In all cases, we checked that the computed H_2 adsorption energies are almost independent of the specific shifted boundary conditions that we used. In the limit of very low H_2 coverage, that is, a single H_2 molecule that splits at a given defect, the characteristics of the formed complexes are mostly influenced by the local conformation of the ions. In contrast, the coadsorption of several H_2 molecules or in the limit of high coverage depends on the defect geometry on a larger scale. For the most stable and representative adsorption configurations, we computed the dynamical matrix and the effective charge tensor within the density functional perturbation theory including up to third neighbors of the H^+, H^- complexes. From these quantities, we determined the mode frequency and eigenvectors, as well as their relative intensities. To compare the computed with experimentally observed OH frequencies, the former ones were rescaled (see Supporting Information).

2.3. Ab Initio Adsorption Free Energy and Pressure. The adsorption energy, ΔE_{ad}, at 0 K for nH_2 molecules has been computed through the difference of the total energy, E_{tot}, of the MgO(ijk) slab with adsorbed H and the sum of the total energies of the clean slab (with the same shifted periodic boundary conditions) and the isolated H_2 molecule as

$$\Delta E_{ad} = E_{tot}(2n\mathrm{H{:}\ MgO}(ijk)) - nE_{tot}(H_{2(gas)}) - E_{tot}(\mathrm{MgO}(ijk)) \quad (1)$$

The molar adsorption energy is then obtained as $\Delta\epsilon_{ad} = \Delta E_{ad}/n$. A large negative $\Delta\epsilon_{ad}$ denotes the stability of the product (the surface with H adatoms) over the reactants (the clean

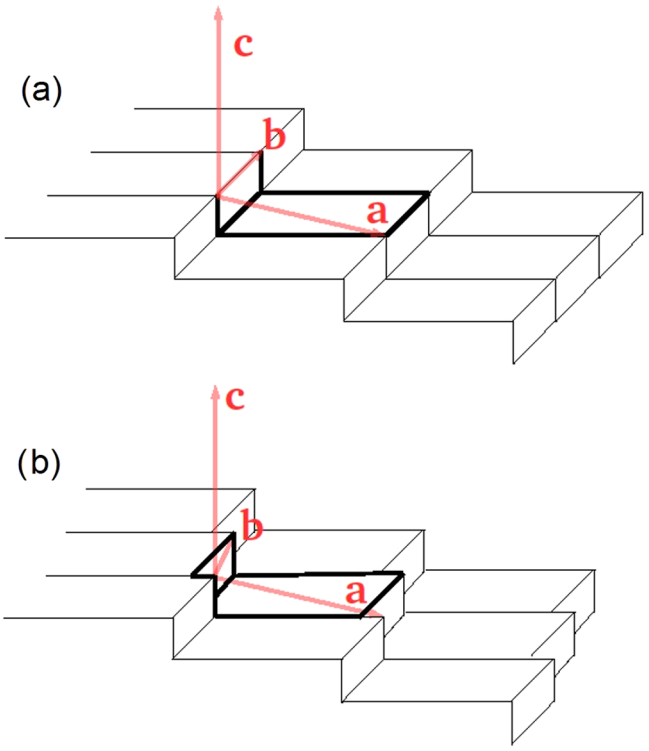

Figure 1. (A) High-index periodic surfaces represented through shifted periodic boundary conditions. Top: shifted periodic boundary conditions for vicinal surfaces with straight steps. In red are shown the base vectors: $a = a_0\ (n_1, 0, -h)$; $b = a_0\ (0, n_2, 0)$; and $c = a_0\ (0, 0, n_3)$. n_1 is the width of the terrace, h the step height in units of the MgO lattice constant a_0. (B) Shifted periodic boundary conditions for vicinal surfaces with kinks. Base vectors: $a = a_0\ (n_1, 0, -h)$; $b = a_0\ (-k, n_2, 0)$; and $c = a_0\ (0, 0, n_3)$. k is the width of the kink on the step in units of the MgO lattice constant a_0. In both cases, we draw only the topmost layer of the periodic surfaces. A thick line represents the repeated unit.

surface and the H_2 molecules in the gas phase). However, one cannot compare this standard procedure directly with experiments, which monitor adsorption as a function of the H_2 partial pressure, P. The pertinent quantity to look at is the Gibbs adsorption free energy, $\Delta g_{ad}(P,T)$, which is the difference between the thermodynamic potentials of products and reactants at a given pressure P and temperature T. $\Delta g_{ad}(P,T)$ can be approximated as

$$\Delta g_{ad}(P, T) = \Delta \varepsilon_{ad} - g_{tra}(P, T) - g_{rot}(P, T) \quad (2)$$

The translational $g_{tra}(P,T)$ and rotational $g_{rot}(P,T)$ contributions to the molar Gibbs free energy of the H_2 molecule in the gas phase were evaluated analytically within the ideal-gas approximation. More details can be found in the Supporting Information.

For any temperature, we define the thermodynamic threshold pressure, P_{ad}, for H_2 dissociative adsorption on the actual surface defect as that for which $\Delta g_{ad}(P_{ad},T) = 0$. Within the previous approximations, P_{ad} reads

$$P_{ad} = (k_B T^2 / 2\Theta\Lambda^3) \exp(\Delta \varepsilon_{ad}/RT) \quad (3)$$

where the characteristic rotational temperature for H_2 is $\Theta \sim 85$ K and $\Lambda = h/(2\pi M k_B T)^{1/2}$ is the thermal wavelength. The computed P_{ad} can then be compared with the onset of H_2 adsorption as experimentally measured, for each adsorption configuration, under the hypothesis that adsorption and desorption of H_2 are mainly governed by thermodynamics. Moreover, we note that an error of 10 kJ/mol (or 0.1 eV/H_2) on the molar adsorption energy, $\Delta \varepsilon_{ad}$, impacts P_{ad} by a factor ~50 at room temperature, which should be thus considered an estimate rather than a precise value.

3. EXPERIMENTAL RESULTS

The TEM image of MgO fabricated by CVS is presented in Figure 2. The powder consists of cubical particles, which

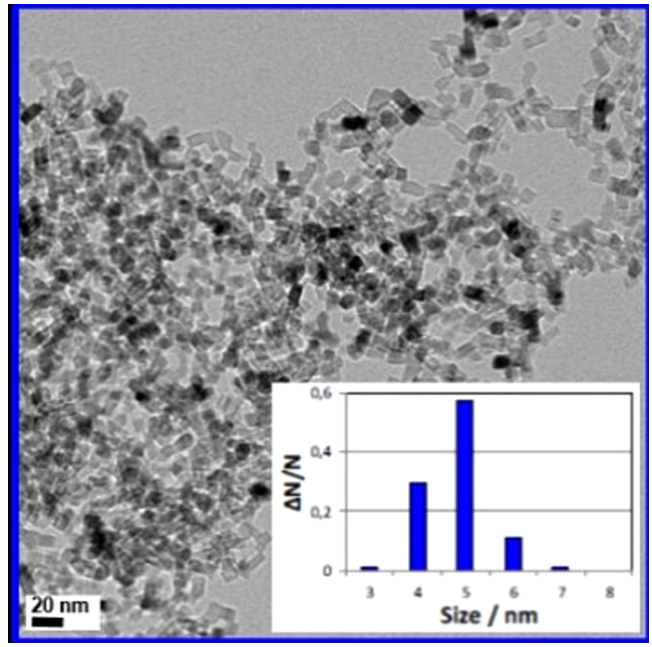

Figure 2. TEM image of MgO nanoparticles. The inset shows the diagram of particle size distribution.

exhibit a quite narrow size distribution of 5 ± 2 nm (inset of Figure 2). In addition, nanocubes appear as an ensemble of particles that share contact lines. These were found to serve as nucleation sites for the growth of metal clusters[19] but also to systematically provide inverse corners, which are often invoked in the chemistry of hydrogen.[9−11] The evolution of IR bands was monitored as a function of the hydrogen partial pressure, P_{H_2}, within the 10^{-8}−100 mbar pressure range. The appearance of infrared bands can be described according to three pressure domains: (i) low (up to 10^{-3} mbar), intermediate (~10^{-3}−1 mbar), and high (>1 mbar) that are indicated in blue, cyan, and green, respectively, in Figure 3.

For the purpose of IR measurements, pellets of 25 mm in diameter were prepared out of 50 mg of MgO powder. Having the specific surface area of ~365 $m^2\ g^{-1}$, it implies that such a pellet equals MgO surface of 15 m^2. Because exposures to hydrogen last 10 min, a pressure of ~2×10^{-5} mbar is required to saturate the pellets, by assuming a fast diffusion of hydrogen. Spectra recorded below 10^{-5} are therefore not quantitatively significant. IR bands at 3712, ~1140 and 863 cm^{-1}, as well as the shoulder at 3697 cm^{-1} are the first that appear. Their intensity grows until the pressure reaches 1 mbar. Thereafter, the saturation limit is reached and no significant changes can be observed regarding the underlined bands. However, when the pressure changes from 10^{-3} mbar, a strong intensity boost is observed for all of these bands along with an appearance of

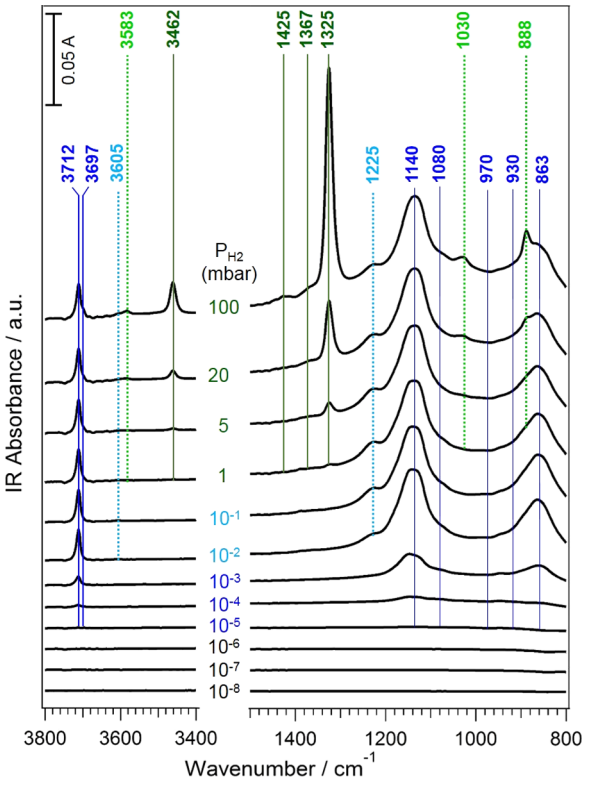

Figure 3. IR spectra of MgO exposed to P_{H_2} = 10^{-8}–100 mbar. Three P_{H_2} regimes can be distinguished: low, <10^{-2} mbar (blue); intermediate, ~10^{-2}–1 mbar (cyan); and high, >1 mbar (green and light green).

new bands at ~3605 and 1225 cm^{-1} (marked cyan in Figure 3) with rather low intensity. The evolution of the band at ~3605 cm^{-1} is shown in Figure S1 (Supporting Information). At P_{H_2} = 1 mbar, bands at 3583, 3462, 1425, 1325, 1030, and 888 cm^{-1} start to grow (marked green in Figure 3), whereas the shoulder at 3697 cm^{-1} increases in intensity.

To probe the stability of the IR bands formed in the presence of hydrogen, the FTIR spectrum obtained after H_2-desorption (P = 10^{-7} mbar) is compared with the one obtained at highest P_{H_2} (Figure 4). All of the species formed below 10^{-3} mbar are irreversibly adsorbed. The intensities of the bands at 3712, 3697, 1139, and 863 cm^{-1} are unaffected by the removal of hydrogen from the gas phase, which is in line with already observed trends.[8] Conversely, all of the features formed under higher H_2 pressures appear to be reversible, except the band at 1030 cm^{-1} that remains stable upon hydrogen removal.

4. SIMULATIONS

The observation of many new IR features with respect to the state of the art, the existence of four pressure regimes instead of two, and the stability in vacuum of a band (1030 cm^{-1}) that appears above 1 mbar, in a pressure range that is expected to give rise to only reversible adsorption, strongly question the current description of the H/MgO system. Simulations were undertaken on a large set of surface H^+/H^- configurations adsorbed on distinct surface defects to find the rationale of the pressure-dependent complexes with different stability. In the atomistic models, both monoatomic and diatomic steps with several surface defects, edges, corners, and inverse corners,

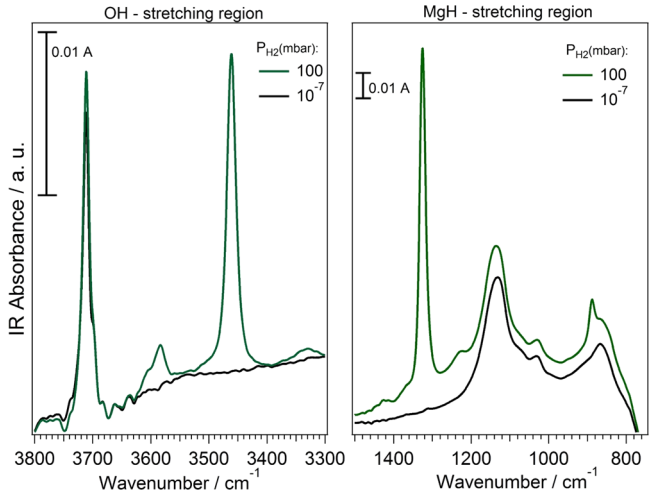

Figure 4. Comparison of the IR spectrum of MgO exposed to P_{H_2} = 100 mbar (green curve) to that obtained at P_{H_2} = 10^{-8} mbar (black curve) after hydrogen desorption.

were considered for a total of about a hundred distinct surface configurations that were all optimized. For the configurations that correspond to negative adsorption energy, the vibrational frequencies were computed within the harmonic approximation.

4.1. Frequencies, Bond Lengths, and Coordination Numbers. The inverse correlation between bond lengths and stretching frequencies has been established in many polyatomic species,[20] solids containing hydroxyls[21] and adsorbed hydroxyls.[22] For a given kind of bond, the shorter the bond, the stiffer it is and, so, the higher the stretching frequency. Our theoretical results confirm the correlation for both O–H (Figure 5a) and H–Mg bonds (Figure 5b). Another important relationship is that bond lengths are increasing functions of the ion coordination numbers.[23,24] As regards hydroxyls, the lower the coordination number of the O^{2-} anion to which the proton binds, the shorter and stronger the OH bond. Typically, the computed OH bond lengths range between 0.970 and 0.975 Å for O_{3C} sites (corners), whereas they are between 0.976 and 0.989 Å for O_{4C} (step edges). The Mg–H bond lengths range between 1.763 and 1.825 Å for Mg_{3C} sites at corners, between 1.786 and 1.920 Å for Mg_{4C} sites at step edges, and between 1.915 and 2 Å for Mg_{5C} sites at terraces.

As a trend, these two correlations enable us to deduce from the measured frequency the types of sites to which H^+ or H^- is bound. However, the presence of other weaker bonds, such as hydrogen bonds or, most importantly, $H_{ads}^{+}\cdots H_{ads}^{-}$ interactions, may affect those robust guidelines, as discussed in Section 4.3.

4.2. Adsorption Enthalpies and Coordination Numbers. The stability of adsorbed groups is directly related to the adsorption enthalpy and thus to the critical pressure, P_{ad}, for H adsorption, as given in eq 3. Adsorption enthalpy can be approximately decomposed into the sum of distinct contributions from the O–H and H–Mg bonds that are created upon H_2 dissociation. However, the simulations provide the sum of these two contributions, which cannot be straightforwardly evaluated as singles. Nevertheless, we could obtain a rough estimate of the relative group stability as follows. For each specific surface conformation (mono- or diatomic steps, and

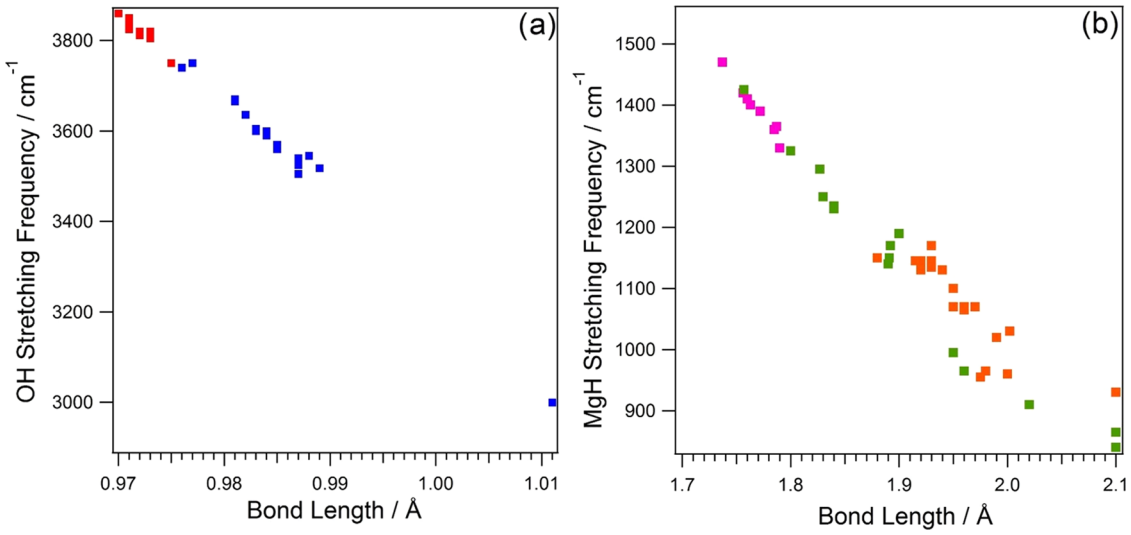

Figure 5. Correlation between computed (a) OH frequencies (not rescaled) and OH bond lengths and (b) MgH frequencies and MgH bond lengths. Squares: red for $O_{3C}H$, blue for $O_{4C}H$, pink for $Mg_{3C}H$, green for $Mg_{4C}H$, and orange for $Mg_{5C}H$.

MgO divacancies in various numbers), we ranged the adsorption configurations from the highest to the lowest stability by increasing computed adsorption enthalpy. For adsorption configurations that differ just by a group (i.e., having either very similar O−H or H−Mg groups), we estimated the difference of the adsorption enthalpies when a group is replaced by another one. In such a way, we extracted the main trends in the relative stability of group subsets.

Regarding hydroxyl groups, adsorption of H^+ on corners is favored relative to step edges, which correlates well with the decreasing O_C−H bond length (Figure 5a). In contrast, the most stable H−Mg configurations are invariably those in which H^- is bound to three Mg cations, where it replaces a missing anion in the network. Then, a finer distinction exists for a similar H^- coordination number but variable Mg coordination number. The rule of thumb to obtain very stable adsorption configurations for H^- is to maximize the number of its bonds to cations having the lowest possible coordination number. As a consequence, the short-range conformation of the surface has an impact on the stability of H−Mg groups: for instance, H binds more tightly at inverse corners on monoatomic ($2Mg_{4C}$ and $1Mg_{5C}$) than at diatomic or polyatomic steps ($3Mg_{5C}$). This trend, which we observed for the heterolytic splitting of H_2, is indeed more general, as monoatomic steps on MgO(001) surfaces are especially reactive toward water.[22,25]

4.3. H^+−H^- Proximity and Diffusion, Kinetics. The proximity of the H^+, H^- fragments that originate from the heterolytic dissociation of H_2 can play a role in the adsorption. Our findings confirm that heterolytic H_2 adsorption is stabilized by the $H^+\cdots H^-$ electrostatic interaction in agreement with ref 9. This opens the question of the role of proximity effects on the thermodynamic stability as well as on stretching frequencies of the OH and MgH groups. The contribution of the stabilizing $H^+\cdots H^-$ interaction can be estimated by comparing the adsorption enthalpies between two adsorption configurations that only differ by d_{HH}. We have studied in detail the three following cases: the monoatomic step (schematized by the (015) surface), the sequence of monoatomic steps (the (011) surface), and the diatomic step (the (026) surface). Overall, the contribution of the electrostatic interaction to the adsorption enthalpy becomes appreciable when the $H^+\cdots H^-$ distance, d_{HH}, is smaller than about 2.0 Å. However, due to limited statistics, we can quantify these effects neither on the adsorption enthalpies nor on the O−H and Mg−H stretching frequencies, but only provide some examples.

The configuration in which the H^+, H^- fragments are far apart is significantly less stable than that in which they are first neighbors. Irrespective of the kind of surface defect that dissociates H_2, the resulting OH and MgH groups are stabilized by the $H^+\cdots H^-$ Coulomb interaction. A paradigmatic case is the monoatomic step. At straight monoatomic steps, the adsorption enthalpy is negative when H^+ and H^- are first neighbors, whereas it is positive whenever the two species are far apart (unstable configuration). As pointed out by Giordano and Pacchioni, H_2 splits in two adjacent $O_{4C}H$ and $Mg_{4C}H$ groups at added atomic rows on MgO(001).[26] Our results on the H_2 splitting at the monatomic step (MgO(015)) confirm their findings and show that the $O_{4C}H$ and $Mg_{4C}H$ groups are stabilized by the $H^+\cdots H^-$ electrostatic interaction, with a remarkable short H^+−H^- bond, d_{HH} = 1.53 Å. The strong $H^+\cdots H^-$ interaction weakens both Mg−H and O−H bonds, stretches the remaining bonds in the MgO network inducing a big distortion of the step, and affects the frequencies: the $O_{4C}H$ group at equilibrium is 1.01 Å long and vibrates at a very low frequency, about 3000 cm^{-1}.

A very important issue in the present context is the role of kinetics in governing H_2 adsorption or diffusion. As far as adsorption is concerned, we found that for several defects it is possible to find a barrierless reaction path, starting from the physisorbed H_2 molecule and ending with split adsorbed H^+ and H^-. This occurs at MgO divacancies on terraces, monoatomic steps, and defects involving an O corner at diatomic steps. Although we did not carry out a systematic study of these reactions, it is reasonable to conclude that all defects involving corners and MgO divacancies are able to dissociate H_2 without activation barrier.

Once H_2 splits into H^+ and H^-, these species remain within the vicinity of the dissociation site unless they are able to diffuse. By increasing the $H^+\cdots H^-$ distance, the attractive Coulomb interaction weakens. Therefore, diffusion is a favorable process only when another more stable adsorption

Table 1. Calculated Frequency ($\tilde{\nu}$), Bond Length (d), Adsorption Enthalpy (ΔH), and Threshold Hydrogen Pressure (P_{H_2}) for the Most Representative Defect Sites[a]

Type of defect	Model Complex	H^+ adsorption site	H^- adsorption site	$\tilde{\nu}_{OH}$ (cm^{-1})	d_{OH}(A)	$\tilde{\nu}_{MgH}$ (cm^{-1})	d_{MgH}(A)	ΔH (eV/H_2) / P_{H_2} (mbar)
A: Mono-atomic step	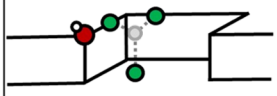	$O^{(3C)}$	2 x Mg $^{(4C)}$ 1 x Mg $^{(5C)}$	3750	0.971	1145; 1020; 965	1.92; 1.99; 2,19	-1.60 <<10^{-8}
B: Di-atomic step	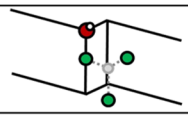	$O^{(3C)}$	1 x Mg $^{(4C)}$ 2 x Mg $^{(5C)}$	3745	0.971	1095; 940; 850	1.935; 2.07; 2,08	-1.35 <<10^{-8}
C: Di-atomic step	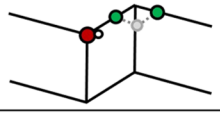	$O^{(3C)}$	2 x Mg $^{(4C)}$	3740	0.971	1140; 905	1.89; 2.02	-0.77 10^{-5}
E: Mono-atomic step	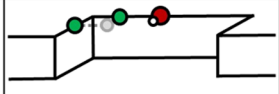	$O^{(4C)}$	2 x Mg $^{(4C)}$	3545	0.982	1190; 930	1.889; 2.10	-0.42 5
F: Mono-atomic step	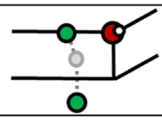	$O^{(3C)}$	1 x Mg $^{(4C)}$ 1 x Mg $^{(5C)}$	3760	0.970	1230; 910	1.88; 2.01	-0.60 10^{-2}
X: Mono-atomic step (X="E+F")	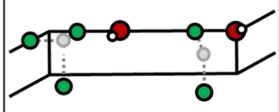	$O^{(4C)}$ $O^{(3C)}$	2x Mg $^{(4C)}$ 1x Mg $^{(5C)}$ 1x Mg$^{(4C)}$ 1x Mg $^{(5C)}$	3510 3760	0.971 0.981	1140; 965 1220; 915	1.888; 1.959 1.877; 2.17	-0.51 10^{-1}
G: Mono-atomic step	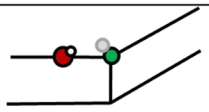	$O^{(4C)}$	1x Mg $^{(3C)}$	3508	0.984	1390	1.771	-0.30 > 100
H:Di-atomic step	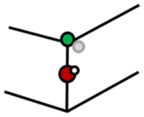	$O^{(4C)}$ (vertical edge)	1x Mg $^{(3C)}$	3480	0.985	1400	1.763	-0.30 > 100
I: Di-atomic step	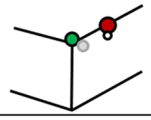	$O^{(4C)}$ (horizontal step edge)	1x Mg $^{(3C)}$	3490	0.984	1410	1.756	-0.32 ~ 50
D: Di-atomic step	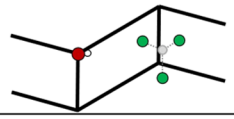	$O^{(3C)}$	3 x Mg $^{(5C)}$	3710	0.971	1105; 1095; 965	1.95, 1.95, 1.98	-0.71 10^{-4}

O^{2-} Mg^{2+} H^+ H^- Crystal Mg-H bond

[a]The color code correlates with that in Figure 3.

configuration is not too far from the dissociation site. For instance, this happens for a kink on a monoatomic step. A sequence of states starting from dissociated $H^+\cdots H^-$ close to the step edge and ending at a neighboring kink site (either O_{3C} or Mg_{3C}) was found. The energy of the configurations along the path between physisorption and dissociation is below the physisorption energy. The barriers along the path could be on the order of 0.3−0.5 eV and are pretty similar to those calculated for the diffusion of atomic H on MgO(001).[27] Therefore, the migration of H^+ or H^- toward more stable configurations (involving O corners or Mg inverse corners) is in principle possible when they are not too far from the reaction site. H_2 dissociation at defects on MgO(001) surfaces is a local or quasi-local process.

We also studied some configurations in which two H_2 molecules split, which could happen at appropriate hydrogen pressures. To the best of our knowledge, such a process, although rather likely, has never been considered in previous works on H_2 splitting at MgO surfaces. The relevance of, as we call, simultaneous or cooperative adsorption will be discussed in relation to experiments in the next chapter.

5. DISCUSSION

We have experimentally observed that IR spectra vary significantly with P_{H_2} and reveal rather complex features.

These, according to their onset and intensity evolution with pressure, can be classified into four P_{H_2} regimes. Their origin is discussed in correlation with surface defects obtained through the simulations. For choosing the best candidate, two main criteria were kept: (i) theoretical P_{H_2} should not much differ from the experimentally observed onset pressure, and (ii) computed frequencies of a given model should match best the IR spectra among all of the candidates. Such a double-check procedure yields an unprecedented and internally consistent classification because the configurations have been obtained independent of the experiments. Configurations that best fit the experimental data are collected in Table 1.

5.1. Adsorption of the Isolated Hydrogen Molecule ($P_{H_2} = 10^{-5}$–10^{-3} mbar). Configurations A–C (Table 1) are among the most stable that we found in the simulations. Including both mono- and diatomic steps on MgO surface, they could form at hydrogen pressures lower than 10^{-4} mbar. Their computed OH (3750–3710 cm^{-1}) and MgH (1145–1095; 965–850 cm^{-1}) stretching frequencies match well with the IR frequencies experimentally observed at the lowest P_{H_2} ($\sim 10^{-5}$ mbar, highlighted in blue in Figure 3). Although rather broad, the main MgH bands are experimentally observed to peak at 1139 and 863 cm^{-1}. By closer inspection, features can be also observed at 1080, 970, and 930 cm^{-1}, in particular, at pressure below 10^{-2} mbar (Figure 3). The calculations may account for the IR data in this frequency range. Configurations A–C involve systematically two components. First, H^+ is adsorbed always on 3-coordinated oxygen (O_{3C}), and the uniqueness of this adsorption site leads to a sharp band at 3712 cm^{-1}. An IR band at 3698 cm^{-1} is also observed. Unlike some reports,[28,29] it cannot be attributed to brucite because such phase transformation cannot be expected under applied experimental conditions. We therefore explain the presence of IR band at 3698 cm^{-1} by configuration C, which is associated with diatomic steps and exhibits a slightly lower frequency than in the case of A and B (Table 1). In the three proposed models, H^- is mainly adsorbed at the Mg inverse corner (Mg_{IC}), in line with configurations previously suggested by other groups.[7−11] In one of these,[11] a configuration similar to our model A (Table 1) is reported. H^- ions are in 3-fold coordination among (100), (010), and (001) faces and give rise to two almost degenerate frequencies (1095–1145 cm^{-1}) corresponding to the shorter and stiffer Mg–H bonds and a lower frequency (850–965 cm^{-1}) associated with the longer and weakest bond. An exception of this rule is represented by model C in which H^- is 2-fold-coordinated after being shared between two edges. However, this model fits this experimental range regarding both, the stability and frequencies.

The intensity of the two bands at 3712 and 1140 cm^{-1} boosts when P_{H_2} increases from 10^{-3} to 10^{-2} mbar. It keeps then increasing softly upon next shot of H_2 (10^{-2}–10^{-1} mbar), whereas it finally saturates at P_{H_2} = 1 mbar, i.e., at the pressure which is several orders of magnitude higher than the onset H_2-pressure (<10^{-5} mbar). This saturation limit was already reported by Diwald et al.,[7,8] but the sudden change in intensity has not been interpreted so far. It cannot rely on thermodynamics because the configurations under study involve the most stable H^+ and H^- adsorption sites, O_{3C} and Mg_{IC}, respectively. Indeed, these sites should be populated at the onset P_{H_2} along with no observable intensity increase, if thermodynamics solely controls adsorption. This is not the case, and we attribute it, rather, to kinetics. Our calculations show that H_2 readily dissociates on neighboring O/Mg sites where H_2 heterolytically splits without barrier. In contrast, the dissociation on more remote O_{3C}/Mg_{IC} sites is hindered by the activation energy of the diffusion of H^+/H^- from one O^{2-}/Mg^{2+} adsorption site to another. Expecting the amount of neighboring O_{3C}/Mg_{IC} to be rather low within the whole set of O corners and Mg inverse corners in the sample, another adsorption mechanism is needed to explain the saturation of the main peaks at medium pressures.

5.2. Cooperative Adsorption ($P_{H_2} = 10^{-3}$–1 mbar). The main change in the IR spectra within the $P_{H_2} = 10^{-3}$–10^{-2} mbar range is the intensity increase of peaks at 3712 cm^{-1} (O_{3C}–H) and at 1140 and 863 cm^{-1} (Mg_{IC}–H) along with the appearance of less intense features at 3605 and 1225 cm^{-1}. Furthermore, band intensities moderately increase up to a hydrogen pressure of 1 mbar (Figure S2). To explain these changes, we invoke the adsorption of two or more H_2 molecules on the basis of "hybrid configurations". These consist of a stable site, such as the $O_{3C}H$ site or $Mg_{IC}H$ accompanied by a less stable site. Examples are given by configurations E and F in Table 1. Besides a $Mg_{IC}H$ site, the former involves an $O_{4C}H$ site whose frequency is calculated at 3545 cm^{-1} i.e., fairly close to the feature observed at 3605 cm^{-1}. In configuration F, the $O_{4C}H$ site is accompanied by a MgH, whose H^- is bound to one Mg on a terrace (Mg_{5C}) and one placed at the vertical edge of a diatomic step (Mg_{4C}). Its frequency, calculated at 1235 cm^{-1}, matches well the feature observed experimentally at 1225 cm^{-1}. However, the occurrence of configurations E and F does not explain the extremely low intensity of the features that appear at 3605 and 1225 cm^{-1}.

Until now, we have discussed the heterolytic splitting of single H_2 molecules on neighboring defects. However, at P_{H_2} = 10^{-3}–10^{-2} mbar, the cooperative absorption has to be considered. The lifetime of a molecule on a surface is $\tau \sim \nu_0^{-1} e^{E_{ads}/RT}$, where $\nu_0 \sim 10$ THz is the attempt frequency, E_{ads} is the adsorption energy, R is the gas constant, and T is the absolute temperature.[30] For E and F configurations, $\tau \sim 10^{-4}$ s by taking $E_{ads} \sim 0.5$ eV (Table 1). On the basis of $\tau \sim 10^{-4}$ s and working at $P_{H_2} \sim 10^{-2}$ mbar, the surface coverage would be close to one monolayer that means one H_2 molecule per surface atom. As a consequence, the probability that another molecule hits the surface close to the first one approaches unity. This suggests that at $P_{H_2} \geq 10^{-3}$ mbar the coadsorption of more than one H_2 molecule is a likely event. Such mechanism is already guessed by Gribov et al.,[11] relying heuristic arguments. The mechanism is examined here thanks to theoretical models consisting of two adsorbed H_2 molecules, such as in configuration X (Table 1) that gathers the above E and F configurations. The calculated frequency and the onset pressures of the X model fit the measured data even better than the previously discussed hybrid configurations. Regarding the stability, the X configuration is calculated to form at 0.8 mbar, which is 2 orders of magnitude above the onset at $P_{H_2} \sim 10^{-3}$–10^{-2} mbar under discussion. However, a typical error of 0.1 eV/H_2 on the adsorption energy could affect the onset pressure by a factor 50 at room temperature so that an error of an order of magnitude is within the present accuracy of most DFT-based calculations. Moreover, the electrostatic attraction between the adsorbed H^- and H^+ on defective surface sites

could slightly increase the absolute adsorption energy and reinforce the stability of the cooperative adsorption.

Most importantly, the X configuration allows the recombination of hydrogen atoms adsorbed on O_{4C} and Mg_{4C}−Mg_{5C} sites, provided they are close enough to react. Indeed, the weak intensity of the features at 3605/1225 cm^{-1} indicates that the recombination is almost the rule and that the desorption process is quite fast. Therefore, the coadsorption of two or more H_2 molecules on hybrid configurations provides an effective mechanism to saturate many stable yet distant O_{3C} and Mg_{IC} sites, which is not possible through direct adsorption of isolated molecules. We stress that, although quite elementary arguments suggest that the surfaces of the nanopowders experience very many interactions with hydrogen per unit time, the coadsorption of several H_2 molecules has never been invoked so far as to quantitatively explain the IR spectra. Such a mechanism could be also at work when dissociating other H-containing molecules over MgO nanopowders, such as CH_4 recently reported by Schwach et al.[31]

5.3. Population of Mg_{3C} Corners (P_{H_2} = 1−100 mbar). IR spectra recorded above 1 mbar (Figure 4, green frame) reveal two prominent and sharp peaks (3460 and 1325 cm^{-1}), the intensity of which promptly increases with pressure.[7,8] Within this P_{H_2} range, the bands at 3712 and 1140−850 cm^{-1} do not vary anymore. Therefore, we can safely assume that the most stable and reactive sites for H_2 splitting (O_{3C} and Mg_{IC}) are completely saturated and other defect sites become responsible for the bands appearing in this P_{H_2} range. According to the above-described trend (Figure 5), the next most reactive O sites toward H^+ must be 4-fold-coordinated, whereas H^- should be coordinated to two or one surface Mg. Because the observed bands are very sharp and intense, well-defined configurations that exist in substantial number on hsa-MgO must lie in their origin. According to our calculations, they were associated with O_{4C} sites, either on monoatomic or diatomic steps, and Mg are sitting in corners (Mg_{3C}) because these sites provide Mg−H stretching frequencies higher than 1300 cm^{-1}. The proposed models are presented in Table 1 and denoted G, H, and I. The frequencies calculated for these models, OH between 3480 and 3510 cm^{-1} and MgH between 1390 and 1410 cm^{-1}, satisfy fairly the experimentally detected bands at 3460 and 1325 cm^{-1} as well as the weak feature observed at 1425 cm^{-1}. Compared to previous cases, agreement between computed and experimentally detected MgH frequencies is slightly less satisfactory; nevertheless, this assignment, in line with previous findings,[12] is perfectly consistent with the sharpness of the experimental peak at 1325 cm^{-1}, which in contrast would be quite a wide band for H bound to Mg_{4C} or Mg_{5C}. According to thermodynamics, there are as many Mg corners as O corners on MgO nanocrystals because the energetics of those defects hardly differs.[17] Therefore, Mg corners must play a role at higher H_2 pressures, where the split molecule is stable. Interestingly, OH bands vibrating at 3576−3547 cm^{-1} were reported together with MgH bands at 1430−1418 cm^{-1} by Gribov et al.[11] In general agreement with the present work, these authors interpreted their observation on the basis of Mg_{3C} configurations to justify the high MgH frequency. However, for the H^+-adsorption site, they suggested an inverse corner formed upon removing a Mg ion so that the proton becomes bonded to three oxygen ions (two O_{4C} and one O_{5C}). According to our simulations, structures similar to those are quite unstable. Indeed, the OH bond length in hydroxyls rarely exceeds 1 Å, which is necessary in such configuration where H^+ replaces a Mg^{2+} ion. In this pressure range, we note also an increase in intensity of the shoulder at 3698 cm^{-1} along with the appearance of additional weak features at 3583, 1030, and 888 cm^{-1}. They are assigned to hybrid structures with frequencies slightly different than those seen at a lower pressure. They would be marginal if a particular behavior of the band at 1030 cm^{-1} did not hold our attention. It is discussed below.

5.4. Desorption (100−10^{-8} mbar). We can see from Figure 4 that, except the band at 1030 cm^{-1}, all IR bands formed under higher H_2 pressures are completely removed upon pumping. In line with previous reports,[8,9] this certainly applies to OH and MgH couple vibrating at 3460 and 1325 cm^{-1}, respectively, but also to all bands involved in hybrid structures (3605−3583/1225 cm^{-1}). The intensity of the 3712/1140/863 cm^{-1} ensemble is essentially unchanged. This demonstrates that the thermodynamically most stable configurations, which include $O_{3C}H$ and $Mg_{IC}H$ parts, remain on the surface upon hydrogen evacuation, even those formed by progressive saturation as pressure increases from 10^{-3} to 1.0 mbar (Figure 3). The very important point to be mentioned is that the stable OH and MgH (irreversible IR bands) mostly result from cooperative adsorption over hybrid configurations, such as X and Y in Table 1.

Finally, although formed above P_{H_2} >1 mbar, the band at 1030 cm^{-1} is stable upon hydrogen removal (Figure 4). This relatively narrow peak is likely related to a well-defined inverse corner that is both able to tightly bind H^- ions and unable to dissociate hydrogen directly so that cooperative adsorption is required. Seen along with the intensity increase of 3698 cm^{-1}, we hypothesize their correlation with multiatomic steps: for instance, the oxygen corner of a multiatomic step ($O_{3C}H$ with 3697 cm^{-1}) and the Mg_{IC} sites at the bottom of the multiatomic step ($Mg_{IC}H$ with 1030 cm^{-1}). The corresponding calculated configuration is represented by model D in Table 1.

To explain desorption trends, we can argue that, at the highest P_{H_2} = 100 mbar, under-coordinated O and Mg sites are highly covered with adsorbed H^+ and H^- species. These progressively desorb as pressure decreases, starting from the less stable sites. In hybrid structures, hydrogen pumping leaves the most stable OH and MgH, namely, $O_{3C}H$ and $Mg_{IC}H$, which became irreversible irrespective of their mutual distance. The different behavior that is observed for adsorption and desorption sequences supports strongly the mechanism that involves hybrid structures and so the cooperative adsorption of two or more H_2 molecules at distinct defects.

5.5. Parallel between Hydrogen and Methane Adsorption on MgO. The nature of the active sites in the oxidative coupling of methane by Li-doped MgO catalysts is vividly debated. Spectroscopic[32] and microscopic analyses[33,34] as well as DFT calculations[35] have questioned the earlier suggestion of Li^+O^- sites.[36] Whereas no paramagnetic resonance was found to evidence Li^+O^- sites,[32] lithium was shown to modify the morphology of MgO. Upon high-temperature treatments, the oxide powder initially dominated by (100) facets exposes an increased population of (110) and (111) facets and low-coordinated sites.[33,34] Active sites of Li-doped MgO are therefore MgO sites, which raises the question of the involvement of corner and step sites.[31,35] Upon exposure

of Li−MgO catalysts to 10 mbar of CH_4, the infrared spectrum of the OH stretching region exhibits bands at 3728, 3680, and 3660 cm^{-1} that are reminiscent of the bands at 3712 and 3697 cm^{-1} observed herein upon the formation of $O_{3C}H$ corner moieties (Figure 3). The involvement of O_{3C} corner sites in the chemisorption of methane on MgO predicted by Kwapien et al. is clearly favored.[35]

6. CONCLUSIONS

In summary, progressive adsorption of hydrogen molecules at the surface of MgO nanocubes was examined by combining IR spectroscopy and DFT simulations. Thermodynamic stability and the distinctive vibrational signatures of an exhaustive set of model configurations have been computed and critically compared with the experimental data obtained at H_2 pressures systematically increased from UHV to near ambient. The use of ultrahigh vacuum was shown to be essential for the identification of the very first adsorption stages. We select several atomistic models that account for the IR data in the various P_{H_2} regimes and explain the onset of H_2 splitting and the progressive saturation of diverse reactive sites. Thermodynamically most stable structures consist of O_{3C} (oxygen at regular corners) and Mg_{IC} (magnesium at inverse corners) and were shown to irreversibly split H_2 molecules in the lowest pressure range (up to 10^{-3} mbar). Our calculations show, however, that whenever H^+/H^- adsorption sites are far apart and not neighbors, the dissociation becomes kinetically hindered, irrespective of the stability of the corresponding adsorption structure. Therefore, the population of distant defect sites at the MgO surface was proposed to proceed via cooperative adsorption of more than one H_2 molecule on hybrid structures combining sites of different reactivity and stability. Such scenario occurs already in the medium range of pressures (10^{-3}−1 mbar) and, then, continues over highest P_{H_2} (1−100 mbar) where the fully reversibly dissociation at Mg_{3C} and O_{4C} sites of mono- and diatomic steps was also detected. The necessity of the coadsorption mechanism is further demonstrated by different adsorption and desorption sequences shown to occur at the involved defect sites. The coadsorption approach, demonstrated to be indispensable for progressive H^+/H^- population of distant defect sites at MgO surfaces, can occur in a wider range of H-containing molecules.

In perspective, the present approach might also affect the issue of hydrogen storage that calls for a deeper understanding of the hydrogen adsorption/desorption cycles at the atomic scale. This would encourage new research efforts on defect engineering and doping of oxide nanopowders with high specific surface area in view of obtaining an alternative to the systems that are presently envisaged for hydrogen storage.

■ ASSOCIATED CONTENT

Supporting Information

The Supporting Information is available free of charge on the ACS Publications website at DOI: 10.1021/acs.jpcc.8b03192.

IR spectra of MgO (Figure S1); Plot of the integral area vs H_2 pressure for the IR bands (Figure S2) (PDF)

■ AUTHOR INFORMATION

Corresponding Author

*E-mail: slavica.stankic@insp.jussieu.fr.

ORCID

Slavica Stankic: 0000-0002-8711-9746

Notes

The authors declare no competing financial interest.

■ REFERENCES

(1) Coluccia, S.; Boccuzzi, F.; Ghiotti, G.; Mirra, C. Evidence for Heterolytic Dissociation of H_2 on the Surface of Thermally Activated MgO Powders. *Z. Phys. Chem.* **1980**, *121*, 141−143.

(2) Ito, T.; Kuramoto, M.; Yoshioka, M.; Tokuda, T. Active Sites for Hydrogen Adsorption on Magnesium Oxide. *J. Phys. Chem.* **1983**, *87*, 4411−4416.

(3) Kobayashi, H.; Yamaguchi, M.; Ito, T. Ab Initio MO Study on Adsorption of a Hydrogen Molecule onto MgO(100) Surface. *J. Phys. Chem.* **1990**, *94*, 7206−7213.

(4) Shluger, A. L.; Gale, J. D.; Catlow, C. R. A. Molecular Properties of the Magnesia Surface. *J. Phys. Chem.* **1992**, *96*, 10389−10397.

(5) Anchell, J. L.; Morokuma, K.; Hess, A. C. An Electronic Structure Study of H_2 and CH_4 Interactions with MgO and Li-Doped MgO Clusters. *J. Chem. Phys.* **1993**, *99*, 6004−6013.

(6) Kobayashi, H.; Salahub, D. R.; Ito, T. Dissociative Adsorption of Hydrogen Molecule on MgO Surfaces Studied by the Density Functional Method. *J. Phys. Chem.* **1994**, *98*, 5487−5492.

(7) Knözinger, E.; Jacob, K.-H.; Hofmann, P. Adsorption of Hydrogen on Highly Dispersed MgO. *J. Chem. Soc., Faraday Trans.* **1993**, *89*, 1101−1107.

(8) Diwald, O.; Hofmann, P.; Knözinger, E. H_2 Chemisorption and Consecutive UV Stimulated Surface Reactions on Nanostructured MgO. *Phys. Chem. Chem. Phys.* **1999**, *1*, 713−721.

(9) Diwald, O.; Sterrer, M.; Knözinger, E. Site Selective Hydroxylation of the MgO Surface. *Phys. Chem. Chem. Phys.* **2002**, *4*, 2811−2817.

(10) Ricci, D.; Di Valentin, C.; Pacchioni, G.; Sushko, P. V.; Shluger, A. L.; Giamello, E. Paramagnetic Defect Centers at the MgO Surface. An Alternative Model to Oxygen Vacancies. *J. Am. Chem. Soc.* **2003**, *125*, 738−747.

(11) Gribov, E. N.; Bertarione, S.; Scarano, D.; Lamberti, C.; Spoto, G.; Zecchina, A. Vibrational and Thermodynamic Properties of H_2 Adsorbed on MgO in the 300-20 K Interval. *J. Phys. Chem. B* **2004**, *108*, 16174−16186.

(12) Cavalleri, M.; Pelmenschikov, A.; Morosi, G.; Gamba, A.; Coluccia, S.; Martra, G. M. Dissociative Adsorption of H_2 on Defect Sites of MgO: A Combined IR Spectroscopic and Quantum Chemical Study. *Stud. Surf. Sci. Catal.* **2001**, *140*, 131−139.

(13) Stankic, S.; Sternig, A.; Finocchi, F.; Bernardi, J.; Diwald, O. Zinc Oxide Scaffolds on MgO Nanocubes. *Nanotechnology* **2010**, *21*, No. 355603.

(14) Giannozzi, P.; Baroni, S.; Bonini, N.; Calandra, M.; Car, R.; Cavazzoni, C.; Ceresoli, D.; Chiarotti, G. L.; Cococcioni, M.; Dabo, I.; et al. Quantum Espresso: A Modular and Open-Source Software Project for Quantum Simulations of Materials. *J. Phys.: Condens. Matter* **2009**, *21*, No. 395502.

(15) (a) Perdew, J. P.; Burke, K.; Ernzerhof, M. Generalized Gradient Approximation Made Simple. *Phys. Rev. Lett.* **1996**, *77*, 3865. (b) Perdew, J. P.; Burke, K.; Ernzerhof, M. Generalized Gradient Approximation Made Simple [Phys. Rev. Lett. 77, 3865 (1996)]. *Phys. Rev. Lett.* **1997**, *78*, 1396.

(16) Kohn, W.; Sham, L. J. Self-Consistent Equations Including Exchange and Correlation. *Phys. Rev.* **1965**, *140*, A1133.

(17) Finocchi, F.; Geysermans, P.; Bourgeois, A. The Role of Hydroxylation in the Step Stability and in the Interaction between Steps: A First-Principles Study of Vicinal MgO Surfaces. *Phys. Chem. Chem. Phys.* **2012**, *14*, 13692−13701.

(18) Ealet, B.; Goniakowski, J.; Finocchi, F. Water Dissociation on a Defective MgO(100) Surface: Role of Divacancies. *Phys. Rev. B* **2004**, *69*, No. 195413.

(19) Stankic, S.; Cortes-Huerto, R.; Crivat, N.; Demaille, D.; Goniakowski, J.; Jupille, J. Equilibrium Shapes of Supported Silver Clusters. *Nanoscale* **2013**, *5*, 2448−2453.
(20) Zavitsas, A. A. Factors affecting the relation between stretching frequencies and bond lengths. Diatomic and polyatomic species without adjustable fitting parameters. *Spectrochim. Acta, Part A* **2015**, *151*, 553.
(21) Szalay, V.; Kovács, L.; Wöhlecke, M.; Libowitzky, E. Stretching Potential and Equilibrium Length of the OH Bond in Solids. *Chem. Phys. Lett.* **2002**, *354*, 56−61.
(22) Finocchi, F.; Hacquart, R.; Naud, C.; Jupille, J. Hydroxyl-Defect Complexes on Hydrated MgO Smokes. *J. Phys. Chem. C* **2008**, *112*, 13226−13231.
(23) Ferraris, G.; Catti, M. Generalization of Baur's Correlations between Bond Strength in Inorganic Structures. *Acta Crystallogr., Sect. B: Struct. Crystallogr. Cryst. Chem.* **1973**, *29*, 2006−2009.
(24) Finocchi, F.; Noguera, C. Structure and Bonding of Small Stoichiometric Lithium Oxide Clusters. *Phys. Rev. B* **1996**, *53*, 4989.
(25) Savio, L.; Smerieri, M.; Orzelli, A.; Vattuone, L.; Rocca, M.; Finocchi, F.; Jupille, J. Common Fingerprint of Hydroxylated non-polar Steps on MgO Smoke and MgO Films. *Surf. Sci.* **2010**, *604*, 252−257.
(26) Chen, H.-Y. T.; Giordano, L.; Pacchioni, G. From Heterolytic to Homolytic H_2 Dissociation on Nanostructured MgO(001) Films as a Function of Metal Support. *J. Phys. Chem. C* **2013**, *117*, 10623−10629.
(27) Wu, G.; Zhang, J.; Wu, Y.; Li, Q.; Chou, K.; Bao, X. Adsorption and Dissociation of Hydrogen on MgO Surface: A First-Principles Study. *J. Alloys Compd.* **2009**, *480*, 788−793.
(28) Martens, R.; Freund, F. The Potential Energy Curve of the Proton and the Dissociation Energy of the OH^- Ion in $Mg(OH)_2$. *Phys. Status Solidi A* **1976**, *37*, 97−104.
(29) Rywak, A. A.; Burlitch, J. M.; Loehr, T. M. Sol-Gel Preparation and Characterization of Magnesium Peroxide, Magnesium Hydroxide Methoxide, and Randomly and (111) Oriented MgO Thin Films. *Chem. Mater.* **1995**, *7*, 2028−2038.
(30) Israelachvili, J. N. *Intermolecular and Surface Forces*, 3rd ed.; Academic Press: Elsevier, 2011.
(31) Schwach, P.; Hamilton, N.; Eichelbaum, M.; Thum, L.; Lunkenbein, T.; Schlögl, R.; Trunschke, A. Structure Sensitivity of the Oxidative Activation of Methane over MgO Model Catalysts: II. Nature of Active Sites and Reaction Mechanism. *J. Catal.* **2015**, *329*, 574−587.
(32) Myrach, P.; Nilius, N.; Levchenko, S. V.; Gonchar, A.; Risse, T.; Dinse, K.-P.; Boatner, L. A.; Frandsen, W.; Horn, R.; Freund, H.-J.; et al. Temperature-Dependent Morphology, Magnetic and Optical Properties of Li-Doped MgO. *ChemCatChem* **2010**, *2*, 854−862.
(33) Zavyalova, U.; Weinberg, G.; Frandsen, W.; Girgsdies, F.; Risse, T.; Dinse, K.-P.; Schloegl, R.; Horn, R. Lithium as a Modifier for Morphology and Defect Structure of Porous Magnesium Oxide Materials Prepared by Gel Combustion Synthesis. *ChemCatChem* **2011**, *3*, 1779−1788.
(34) Luo, L.; Jin, Y.; Pan, H.; Zheng, X.; Wu, L.; You, R.; Huang, W. Distribution and Role of Li in Li-Doped MgO Catalysts for Oxidative Coupling of Methane. *J. Catal.* **2017**, *346*, 57−61.
(35) Kwapien, K.; Paier, J.; Sauer, J.; Geske, M.; Zavyalova, U.; Horn, R.; Schwach, P.; Trunschke, A.; Schloegl, R. Sites for Methane Activation of Lithium-Doped Magnesium Oxide Surfaces. *Angew. Chem., Int. Ed.* **2014**, *53*, 8774−8778.
(36) Lunsford, J. H. The Catalytic Oxidative Coupling of Methane. *Angew. Chem., Int. Ed.* **1995**, *34*, 970−980.